The effect of 1′,3,5,5′-tetramethyl-1′H-1,3′-bipyrazole on the corrosion of steel in 1.0 M hydrochloric acid

K. Tebbji · H. Oudda · B. Hammouti ·
M. Benkaddour · S. S. Al-Deyab · A. Aouniti ·
S. Radi · A. Ramdani

Abstract The effect of some prepared compounds, namely 3,5-dimethyl-1H-pyrazole (P1), 3(5)-amino-5(3)-methylpyrazole (P2), and 1′,3,5,5′-tetramethyl-1′H-1,3′-bipyrazole (P3), on the corrosion behaviour of steel in 1.0 M hydrochloric acid solution as corrosive medium has been investigated at 308 K using weight-loss measurement, potentiodynamic polarisation, linear polarisation, and impedance spectroscopy (EIS). Generally, inhibition efficiency of the investigated compounds was found to depend on the concentration and nature of the inhibitor. P3 was a better inhibitor than P1 and P2, and its inhibition efficiency increased with increasing concentration of inhibitor, attaining 94% above 10^{-3} M. Potentiodynamic polarisation studies clearly reveal that P3 acts essentially as a cathodic inhibitor. E (%) values obtained from different methods are in reasonably good agreement. EIS measurements show an increase of transfer resistance with inhibitor concentration. Partial π-charge on atoms was calculated. Correlation between the

K. Tebbji · B. Hammouti (✉) · M. Benkaddour · A. Aouniti · A. Ramdani
LCAE-URAC180, Faculté des Sciences, Université Mohammed Premier, B.P. 717, Oujda, Morocco
e-mail: hammoutib@yahoo.fr

H. Oudda
Laboratoire des Procédés de Séparation, Faculté des Sciences, Université Ibn Tofail,
Kenitra, Morocco

S. S. Al-Deyab
Chemistry Department, College of Science, King Saud University, 2455, Riyadh 11451,
Saudi Arabia

S. Radi
LCOMPN-URAC 25, Faculté des Sciences, Université Mohammed Premier, B.P. 717,
Oujda, Morocco

highest occupied molecular orbital energy E_{HOMO} and inhibition efficiencies was sought. The temperature effect on the corrosion behaviour of steel in 1.0 M HCl without and with different concentrations of inhibitor P3 was studied in the temperature range 308 to 343 K. Thermodynamic data, for example heat of adsorption (ΔH°_{ads}), entropy of adsorption (ΔS°_{ads}) and free energy of adsorption (ΔG°_{ads}) were calculated by use of thermodynamic equations. Kinetic activation data, for example E_a, ΔH^*, ΔS^* and pre-exponential factor, were calculated, and are discussed. The inhibiting action of P3 on the corrosion of steel in 1–10 M hydrochloric acid was also studied by weight-loss measurement. The rate constant and reaction constant were calculated for the corrosion reactions. Adsorption of P3 on the steel surface in 1.0 M HCl follows the Langmuir isotherm model.

Keywords   Pyrazole · Steel · Hydrochloric acid · Corrosion inhibition · Adsorption

Introduction

Aqueous solutions of acids are among the most corrosive media. So, the rate of corrosion at which metals are destroyed in acidic media is very high, especially when soluble corrosion products are formed. Acid solutions are generally used in several processes, for example industrial cleaning, acid descaling, and petrochemical processes. Hydrochloric acid is widely used in the pickling processes of metals. The use of inhibitors is one of the most practical methods for protection against corrosion, especially in acidic media [1].

The corrosion inhibition of metal may involve either physisorption or chemisorption of the inhibitors by the metal surface and subsequent interference with either cathodic or anodic reactions, or both, occurring at the adsorption sites.

Most of the well-known acid inhibitors are organic compounds containing nitrogen, sulfur, or oxygen atoms. Nitrogen-containing compounds function more effectively in HCl [2, 3], whereas sulfur-containing compounds are sometimes preferred for H_2SO_4. The effect of organic compounds containing both nitrogen and sulfur atoms have been investigated by several authors [4–7].

It is well known that pyrazole [8–10], bipyrazole [11–16], tripyrazole [17], triazole [18–20] and tetrazole [5, 21] derivatives are excellent inhibitors of corrosion of many metals and alloys in aggressive media. Substitution in the pyrazole ring (R = H, CH_3, $CO_2C_2H_5$, etc.) has a pronounced effect on inhibition efficiency.

The objective of this was to study the effect of some pyrazole derivatives, for example 3,5-dimethyl-1*H*-pyrazole (P1), 3(5)-amino-5(3)-methylpyrazole (P2) and 1′,3,5,5′-tetramethyl-1′*H*-1,3′-bipyrazole (P3), as corrosion inhibitors for steel in molar hydrochloric acid solution. The behaviour of steel in 1.0 M HCl with and without inhibitor was studied using gravimetric, potentiodynamic, and EIS measurements. These results are complemented with theoretical calculations in order to provide an explanation of the differences between the inhibitors.

Experimental

Synthesis of the pyrazole compounds

Compounds P1 and P2 are commercially available. Product P3 was prepared, as previously described [22, 23], from 3(5)-amino-5(3)-methylpyrazole P2 by diazotation in HCl followed by reduction with tin chloride and condensation with beta-diketones. Finally, the methylation of the precursor in the presence of *t*-BuOK as base led to one isolated isomer of P3 in good yield. The molecular structures are shown in Scheme 1.

Gravimetric, R_p, polarisation and EIS measurements

The aggressive solution (1.0 M HCl) was prepared by dilution of analytical-grade 37% HCl with double-distilled water. Before all measurements, the steel samples (0.09% P; 0.38% Si; 0.01% Al; 0.05% Mn; 0.21% C; 0.05% S and the remainder iron) were polished with different emery paper up to 1200 grade, washed thoroughly with double-distilled water, degreased with AR-grade ethanol and acetone, and dried at room temperature.

Gravimetric measurements were carried out in a double-walled glass cell equipped with a thermostated cooling condenser. The solution volume was 100 mL. The steel specimens used were rectangular in shape (2.5 cm × 2 cm × 0.05 cm). The immersion time for weight-loss measurement was 6 h at 308 K. After the corrosion test, the specimens of steel were carefully washed in double-distilled water, dried and then weighed. The rinse removed loose segments of the film from the corroded samples. Duplicate experiments were performed in each case and the mean value of the weight loss is reported. Weight loss enabled us to calculate the mean corrosion rate, expressed in mg cm^{-2} h^{-1}.

Electrochemical measurements were carried out in a conventional three-electrode cylindrical Pyrex glass electrolysis cell. The working electrode (WE) in the form of a disc cut from steel has a geometric area of 1 cm^2 and is embedded in polytetrafluoroethylene (PTFE). A saturated calomel electrode (SCE) and a disc platinum electrode were used as reference and auxiliary electrodes, respectively. The temperature was thermostatically controlled at 308 ± 1 K. The WE was abraded with silicon carbide paper (grade P1200), degreased with AR-grade ethanol and acetone, and rinsed with double-distilled water before use.

Running on an IBM compatible personal computer, the 352 Soft Corr III Software communicates with EG&G Instruments Potentiostat–Galvanostat model
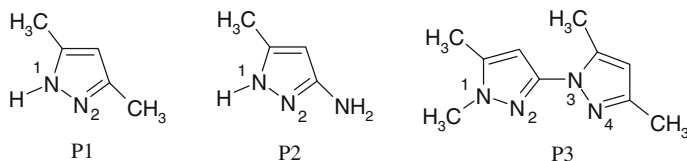
Scheme 1 Chemical formulas of the compounds used

263A at a scan rate of 0.5 mV/s. Before recording the cathodic polarisation curves, the steel electrode was polarised at −800 mV for 10 min. For anodic curves, the potential of the electrode was swept from its corrosion potential, after 30 min at free corrosion potential, to more positive values. The test solution was de-aerated with pure nitrogen. Gas bubbling was maintained throughout the experiments.

Near E_{corr}, a scan through a potential range was used to perform polarisation resistance measurements. The potential range was ±10 mV around E_{corr}. The resulting current was plotted against potential. Polarisation resistance (R_p) values were obtained from the current potential plot. The scan rate was 0.05 mV/s.

The electrochemical impedance spectroscopy (EIS) measurements were carried out with an electrochemical system (Tacussel) which included a digital potentiostat model Voltalab PGZ 100 computer. At E_{corr}, after immersion in solution without bubbling, the circular surface of steel exposing 1 cm^2 to the solution was used as working electrode. After determination of the steady-state current at a given potential, a sine wave voltage (10 mV) peak to peak, at frequencies between 100 kHz and 10 mHz, was superimposed on the rest potential. Computer software automatically controlled the measurements performed at rest potentials after 30 min of exposure. The impedance diagrams are given in the Nyquist representation. Values of R_t and C_{dl} were obtained from Nyquist plots.

Results and discussion

Weight loss tests

Gravimetric measurements of steel subjected to the effects of 1.0 M HCl in the absence and presence of various concentrations of pyrazole derivatives were made after 6 h of immersion at 35 °C. The inhibition efficiency (E_W, %) was calculated by use of the equation:

$$E_w\% = \frac{W_{corr} - W_{corr}^{inh}}{W_{corr}} \times 100 \tag{1}$$

where W_{corr} and W_{corr}^{inh} are the corrosion rates of steel in the absence and presence, respectively, of the organic compound.

According to Table 1, for P1, P2 and P3, the rate of corrosion of steel decreased with increasing inhibitor concentration. The E_w (%) values increased with increasing inhibitor concentration. At 10^{-3} M for each inhibitor studied, the inhibition efficiency attained 36, 55 and 94%, respectively, for P1, P2 and P3. From weight loss measurements, we can conclude that the inhibition efficiency of three pyrazole compounds tested follow the order: P3 > P2 > P1. It can be noted that at concentrations lower than 10^{-5} M, P1 can be regarded as a corrosion stimulator.

We remark that substitution of a methyl (–CH$_3$) of the pyrazole molecule (P1) by an amino group (–NH$_2$) increased the inhibition efficiency of inhibitor (P2). Whereas we note that the presence of two pyrazole rings in inhibitor (P3) substantially increased the inhibition efficiency of this inhibitor.

Table 1 Gravimetric results of steel in acid without and with addition of P1, P2 and P3

Inhibitor	Concentration (M)	W (mg cm^{-2} h^{-1})	E_w (%)
Blank	1	1.06	–
P1	10^{-6}	1.105	−4
	10^{-5}	1.095	−3
	5×10^{-5}	0.952	10
	10^{-4}	0.772	27
	5×10^{-4}	0.698	34
	10^{-3}	0.676	36
P2	10^{-6}	1.026	3
	10^{-5}	1.001	6
	5×10^{-5}	0.829	22
	10^{-4}	0.694	35
	5×10^{-4}	0.515	51
	10^{-3}	0.479	55
P3	10^{-6}	0.994	6
	10^{-5}	0.768	28
	5×10^{-5}	0.376	65
	10^{-4}	0.295	72
	5×10^{-4}	0.103	90
	10^{-3}	0.068	94

It is interest to note that the inhibiting effect of P3 can be attributed to its adsorption at the metal–solution interface, owing to the presence of many active centres (several nitrogen atoms and many π-electrons of the pyrazole rings) for adsorption.

Polarisation measurements

Evaluation of E (%) can also be performed via electrochemical experiments which consist of determination of intensity/potential curves. Cathodic and anodic polarisation curves for steel in 1.0 M HCl in the presence of 10^{-3} M P1, P2 and P3 at 308 K are shown in Fig. 1. In the cathodic domain, it is clear that the current density decreases with addition of pyrazole compounds; this indicates that these compounds are adsorbed on the metal surface and hence inhibition occurs.

At the same concentration (10^{-3} M), the value of I_{corr} of steel for P3 is smaller than those of P1 and P2. P3 results in more efficient inhibition than P1 and P2 in 1.0 M HCl; this enhanced efficiency is because of the presence of the two pyrazole rings in molecule P3. The polarisation study confirms the excellent inhibiting character of P3 obtained with weight loss measurements.

In order to better understand the mechanism of inhibition of P3, a detailed study of this compound was carried out. Polarisation curves for steel at various concentrations of P3 in de-aerated normal HCl solutions are shown in Fig. 2. Electrochemical data, including corrosion potential (E_{corr}), corrosion current density (I_{corr}), and cathodic Tafel slopes (β_c) calculated by use of Tafel fit, are listed in Table 2.
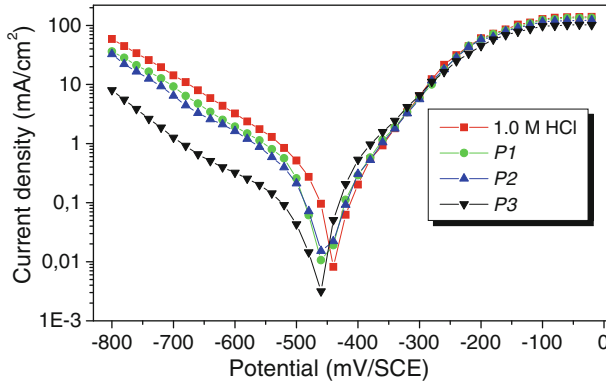
Fig. 1 Polarisation curves of steel in 1.0 M HCl without and with 10^{-3} M P1, P2 and P3
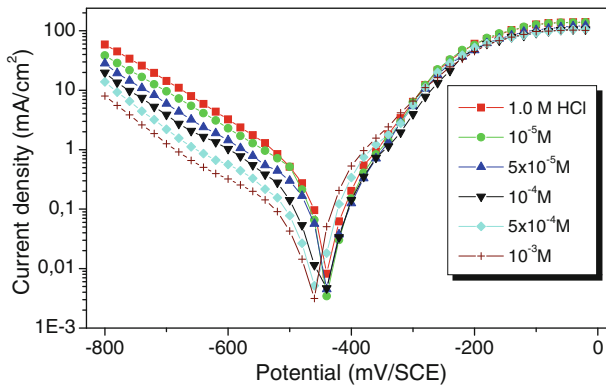

Fig. 2 Polarisation curves of steel in 1.0 M HCl containing different concentrations of P3

Table 2 Electrochemical data for steel at different concentrations of P1, P2 and P3 studied in 1 M HCl, and the corresponding corrosion inhibition efficiencies

Inhibitor	Concentration (M)	E_{corr} (mV/SCE)	β_c (mV/dec)	I_{corr} (μA/cm^2)	E_I (%)	R_P (Ω cm^2)	E_{R_P} (%)
Blank	1	-445	153	305	–	68	–
P1	10^{-3}	-449	155	201	34	98	31
P2	10^{-3}	-450	154	159	48	123	45
P3	10^{-6}	-443	158	281	8	76	11
	10^{-5}	-446	163	244	20	90	24
	5×10^{-5}	-444	156	129	58	168	60
	10^{-4}	-448	158	102	67	187	64
	5×10^{-4}	-452	149	52	83	381	82
	10^{-3}	-460	151	35	89	517	87

Inhibition efficiency (E_I %) can also be calculated from polarization tests by using the following equation:

$$E_I\% = \frac{I_{corr} - I_{corr}^{inh}}{I_{corr}} \times 100 \qquad (2)$$

where I_{corr} and I_{corr}^{inh} are the corrosion current density values without and with the inhibitor, respectively, determined by extrapolation of cathodic Tafel lines to the corrosion potential.

It is clear that addition of P3 hinders acid attack on the steel electrode and comparison of the curves shows that, relative to the blank, increasing the concentration of the inhibitor gave rise to a consistent decrease of cathodic current densities (Fig. 2). As is shown in Fig. 2, the cathodic current–potential curves give rise to parallel Tafel lines, which indicate that the hydrogen evolution reaction is activation-controlled and that addition of the P3 does not modify the mechanism of this process [5].

The analysis of these data shows that:

- the values of I_{corr} of steel in the inhibited solutions were smaller than that for the inhibitor-free solution in 1.0 M hydrochloric acid;
- addition of P3 modifies E_{corr} values slightly, and moves them toward negative potentials, and we notice that the inhibition efficiency increased with inhibitor concentration reaching a maximum value at 10^{-3} M P3. The corresponding efficiency values are 89% in 1.0 M HCl;
- addition of P3 to the corrosive solution causes slight modification of the cathodic slope of the Tafel line (β_c); for example, for 10^{-3} M P3 in 1.0 M HCl solution, the concentration for which the current densities are weakest, β_c equals 176 mV dec^{-1} which is very near of the value obtained in the reference case (153 mV dec^{-1}). This result suggests that the mechanism of hydrogen reduction on the surface of steel is not modified by addition of P3;
- the anodic curves indicate that the mode of inhibition of organic compounds depends on electrode potential (Figs. 1, 2). It seems that the presence of the three inhibitors does not change the current versus potential characteristics. These results indicate that the molecules tested act essentially as cathodic inhibitors.

The corresponding polarisation resistance (R_P) values of steel in 1.0 M HCl in the absence and presence of different concentrations of the inhibitor (P3) are also given in Table 2. R_P was determined by the slope of the potential versus current lines.

We remark that R_P increases with increasing inhibitor concentration. This in turn leads to a decrease in I_{corr} values. The inhibition efficiency (E_{R_P} %) from the linear polarization technique is calculated as follows:

$$E_{R_P}\% = \frac{R_p' - R_p}{R_p'} \times 100 \qquad (3)$$

R_p and R_p' are the polarisation resistance in the absence and presence, respectively, of the inhibitor.

From Table 2, we notice that the E_{R_P} (%) increased with inhibitor concentration reaching a maximum value of 87% at 10^{-3} M for P3. This is in reasonably good agreement with the value of inhibitor efficiency obtained from polarisation (89%) and weight-loss (94%) measurements.

Effect of the concentration of the P3 inhibitor on the rate of corrosion of steel and on inhibition efficiency at different temperatures

Different experimental techniques can be used to evaluate corrosion rate and inhibition efficiency of P3 inhibitor in 1.0 M HCl. The weight loss method is one of the simplest.

To study the relationship between corrosion rate of steel in the absence and presence of P3 molecule, experiments were carried out in the concentration range of P3 from 10^{-5} to 10^{-3} M in 1.0 M hydrochloric acid. Moreover, to investigate the effect of temperature on the corrosion rate of steel, experiments at different temperatures were performed.

The curves showing the values of corrosion rate in the absence and the presence of different concentrations of P3 at different temperatures are drawn in Fig. 3. It is evident that steel corrosion is reduced by the presence of P3 in 1.0 M hydrochloric acid, and the corrosion rate gradually decreases with increasing inhibitor concentration at each experimental temperature, which means that a good inhibition effect can be provided at a higher inhibitor concentration. It is also obvious that in the absence and presence of P3, the corrosion rate of steel increases with increasing temperature.

The values of inhibition efficiencies obtained from the weight loss for different concentrations of P3 at different temperatures in hydrochloric acid are given in Table 3.

It can be seen from Fig. 4 and Table 3 that inhibition efficiency increases with increasing inhibitor concentration, and decreases with increasing experimental
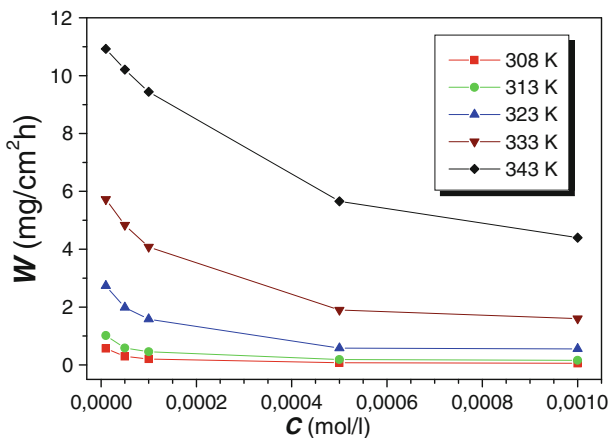

Fig. 3 The relationship between corrosion rate and the concentration of the inhibitor P3

Table 3 Inhibition efficiencies obtained from the corrosion rate for different concentrations of P3 in 1.0 M HCl at different temperatures

Inhibitor P3	Inhibition efficiency (E_w %)				
	308 K	313 K	323 K	333 K	343 K
10^{-5}	34	25	10	5	2
5×10^{-5}	66	57	35	20	8
10^{-4}	76	66	48	32	15
5×10^{-4}	91	86	81	68	49
10^{-3}	93	88	82	73	60
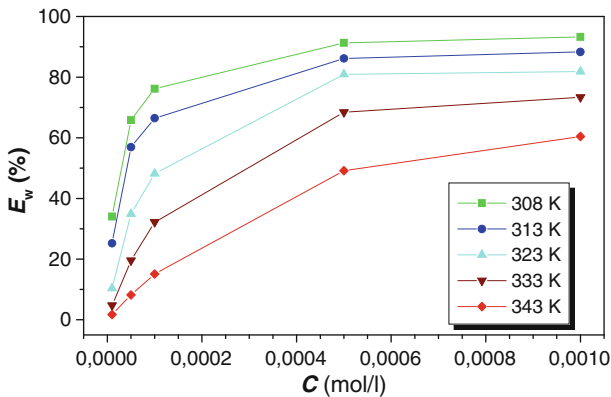
Fig. 4 Relationship between inhibition efficiency and concentration of P3 in 1.0 M HCl

temperature, which suggests that inhibition of the corrosion of steel by P3 might be caused by adsorption of P3 on to the steel surface from acidic solution. So higher temperature might cause desorption of P3 from the steel surface.

Adsorption isotherm and thermodynamic data

For organic inhibitors that have the ability to adsorb strongly on metal surface, thus impeding the dissolution reaction, the surface coverage (θ) can be evaluated as the inhibition efficiency (E_w %/100) [24]. Surface coverage values for the bipyrazole compound P3 have been obtained from the gravimetric weight loss measurements for various concentrations as reported in Table 3.

Adsorption isotherms are very important for determining the mechanism of organic electrochemical reactions. This process is closely related to adsorption of the inhibitor molecules [25, 26] and adsorption is known to depend on chemical structure [27–30].

The most frequently used adsorption isotherms are the Langmuir, Temkin and Frumkin isotherms with the general formula:

$$f(\theta, x)\, e^{-2a\theta} = K_{ads}\, C \tag{4}$$

In hydrochloric acid solution, the organic compound follows the Langmuir adsorption isotherm. This is as follows:

$$\frac{\theta}{1 - \theta} = K_{ads} + C \tag{5}$$

Rearranging this equation gives:

$$\frac{C}{\theta} = \frac{1}{K_{ads}} + C \tag{6}$$

where C is the concentration of inhibitor, K_{ads} is the adsorptive equilibrium constant, and θ is the surface coverage.

From the values of surface coverage, the linear regressions between C/θ and C were calculated by the computer, and the adsorption coefficients, slopes, and linear correlation coefficients are listed in Table 4. Figure 5 shows the relationship between C/θ and C at different temperatures. These results show that all the linear correlation coefficients (r) are almost equal to 1.000 and all the slopes are very close

Table 4 Parameters of the linear regression between C/θ and C for P3

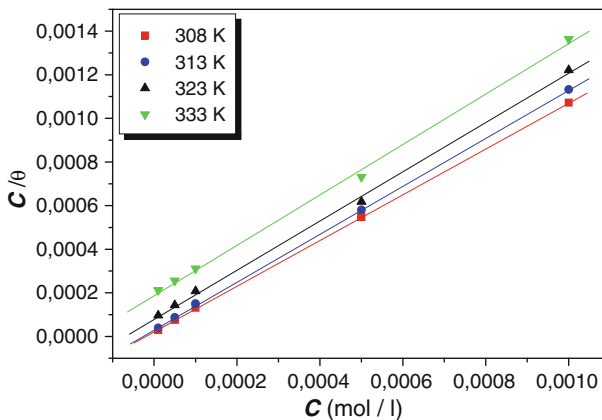| Temperature (K)	Linear regression coefficient (r)	K_{ads}	Slope	ΔS°_{ads} (kJ mol^{-1})	ΔH°_{ads} (kJ mol^{-1})	ΔS°_{ads} (J mol^{-1} K^{-1})
308	0.9999	43950.64	1.04	−37.688	−79.142	−134.591
313	0.9999	29894.56	1.09	−37.296	−79.142	−133.693
323	0.9994	11920.73	1.12	−36.017	−79.142	−133.514
333	0.9990	5217.25	1.15	−34.843	−79.142	−133.030
343	0.9967	1830.72	1.07	−32.901	−79.142	−134.813

Fig. 5 The relationship between C/θ and C for P3

to 1.00, which indicates that adsorption of inhibitor on to the steel surface accords with the Langmuir adsorption isotherm.

Furthermore, it was found (Table 4) that the adsorption coefficient (K_{ads}) decreased with increasing temperature. It is well known that K_{ads} indicates the adsorption power of the inhibitor on to the steel surface; clearly, P3 gave high values of K_{ads} at low temperatures, indicating that it was adsorbed strongly on to the steel surface. Thus, the inhibition efficiency decreased with increasing temperature as the result of increased desorption of P3 from the steel surface.

The corrosion inhibition of P3 for steel could be well explained by using a thermodynamic model, so, the adsorption heat, the adsorption free energy, and the adsorption entropy were calculated to elucidate the phenomenon for the inhibitive action of P3.

According to the Van't Hoff equation [31, 32]:

$$\ln{(K_{ads})} = -\frac{\Delta H_{ads}^{\circ}}{RT} + \text{Constant} \tag{7}$$

where ΔH_{ads}° and K_{ads} are the heat of adsorption and adsorptive equilibrium constant, respectively.

To obtain the heat of adsorption, the linear regression between $\ln{(K_{ads})}$ and $1/T$ was studied; this relationship is shown in Fig. 6. Under these experimental conditions, the adsorption heat could be approximately regarded as the standard heat of adsorption (ΔH_{ads}°) [32, 33]. The standard free energy of adsorption (ΔG_{ads}°) was obtained by use of the equation [34]:

$$K_{ads} = \frac{1}{55.5}\, e^{-\frac{\Delta G_{ads}^{\circ}}{RT}} \tag{8}$$

where 55.5 is the molar concentration of water in solution, in mol L^{-1}.

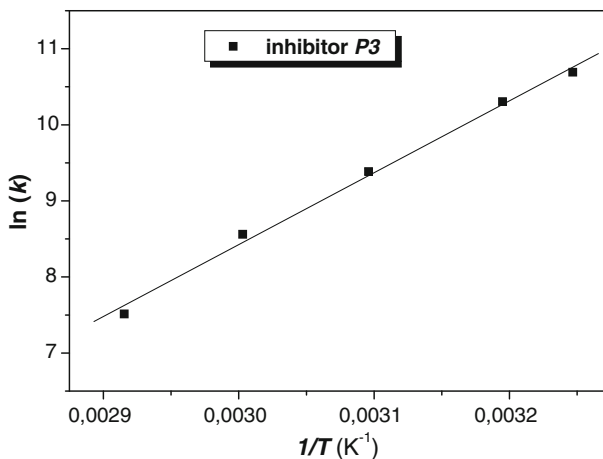
Fig. 6 The relationship between $\ln{(K_{ads})}$ and $1/T$

According to the basic thermodynamic equation $\Delta G^{\circ}_{ads} = \Delta H^{\circ}_{ads} - T\Delta S^{\circ}_{ads}$, the standard entropy of adsorption ΔS°_{ads} could be calculated. Adsorption equilibrium constants K_{ads} and other thermodynamic data for the adsorption process that were obtained from Fig. 6 are summarized in Table 4.

It was found that ΔG°_{ads} increased with increasing temperature (it was more difficult for P3 to be adsorbed on to the steel surface); this phenomenon once again indicated that the adsorption was unfavourable with increasing experimental temperature as the result of the desorption of inhibitor from the steel surface. The negative values of ΔG°_{ads} (Table 4) ensure the spontaneity of the adsorption process and the stability of the adsorbed layer on the steel surface. Generally, values of ΔG°_{ads} up to −20 kJ/mol are consistent with the electrostatic interaction between the charged molecules and the charged metal (physisorption) whereas those around −40 kJ mol^{-1} or higher are associated with chemisorption as a result of sharing or transfer of electrons from organic molecules to the metal surface to form a coordinate type of bond (chemisorption) [35, 36]. One can see that the calculated ΔG°_{ads} values range from approximately −37.688 to −32.901 kJ mol^{-1}, indicating, therefore, that the mechanism of adsorption of the P3 on steel in 1.0 M HCl solution was typical of chemisorption (Table 4).The possible mechanisms of chemisorption can be attributed to donation of π-electrons by the pyrazole rings, and the presence of nitrogen atoms in the pyrazole molecule as reactive centres.

The values of the thermodynamic data for the adsorption of inhibitors can provide valuable information about the mechanism of corrosion inhibition. The endothermic adsorption process ($\Delta H^{\circ}_{ads} > 0$) is attributed unequivocally to chemisorption [37]. Generally, an exothermic adsorption process ($\Delta H^{\circ}_{ads} < 0$) may involve either physisorption or chemisorption or a mixture of both. In an exothermic process, physisorption is distinguished from chemisorption because the absolute value of a physisorption process is lower than 41.86 kJ mol^{-1} whereas the heat of adsorption of a chemisorption process approaches 100 kJ mol^{-1} [38].

In this case; the negative sign of ΔH°_{ads} indicates that adsorption of inhibitor molecules is an exothermic process [39]. A absolute value of ΔH°_{ads} (79.142 kJ mol^{-1}) for adsorption of the inhibitor P3 is approaching 100, so we can also confirm that the adsorption mechanism of P3 on steel in 1.0 M HCl solution was typical chemisorption. Usually, adsorption at a surface involves reduction of translational degrees of freedom (i.e., $\Delta S^{\circ}_{ads} < 0$) as was observed in this investigation (Table 4).

In order to confirm the result of the standard heat of adsorption ($\Delta H^{\circ}_{ads} = -79.142$ kJ mol^{-1}) found from the Van't Hoff equation (eq. 7) we also calculated it by use of Gibbs–Helmholtz equation, which is defined as follows:

$$\left[\frac{\partial(\Delta G^{\circ}_{ads}/T)}{\partial T}\right]_P = -\frac{\Delta H^{\circ}_{ads}}{T^2} \tag{9}$$

This equation can be arranged to give the equation.

$$\frac{\Delta G^{\circ}_{\text{ads}}}{T} = \frac{\Delta H^{\circ}_{\text{ads}}}{T} + A \tag{10}$$

The variation of $\Delta G^{\circ}_{\text{ads}}/T$ with $1/T$ gives a straight line with a slope that equals $\Delta H^{\circ}_{\text{ads}}$ (Fig. 7). It can be seen from the figure that $\Delta G^{\circ}_{\text{ads}}/T$ decreases with $1/T$ in a linear fashion. The value of $\Delta H^{\circ}_{\text{ads}}$ is negative ($\Delta H^{\circ}_{\text{ads}} = -79.142$ kJ mol^{-1}), reflecting the exothermic behaviour of adsorption on the steel surface.

The value of the enthalpy of adsorption found by the two methods, Van't Hoff and Gibbs–Helmholtz, are in very good agreement.

Kinetic parameters

In order to obtain the effect of the inhibitor on the kinetic data, gravimetric weight loss experiments were conducted at 35, 40, 50, 60, and 70 °C in 1.0 M HCl after 1 h of immersion in the absence and presence of P3 at different concentrations. The activation data for the system: the activation energy, enthalpy, and entropy (E_a, ΔH^* and ΔS^*), were calculated from Arrhenius-type plots (eq. 11) and transition state equation (eq. 12) [40].

$$W = A e^{-\left(\frac{E_a}{RT}\right)} \tag{11}$$

where E_a represents the apparent activation energy, R the gas constant, T the absolute temperature, A the pre-exponential factor, and W the corrosion rate.

$$W = \frac{RT}{N_A h} e^{-\left(\frac{\Delta S^*}{R}\right)} e^{-\left(\frac{\Delta H^*}{RT}\right)} \tag{12}$$

where h is Planck's constant, N_A is Avogadro's number, R the universal gas constant, ΔH^* the enthalpy of activation, and ΔS^* the entropy of activation.

A plot of ln W versus $1/T$ gave straight lines with correlation coefficients (r) in the range 0.9962–0.9992 (average: 0.9973), and slope $-E_a/R$, as shown in Fig. 8.
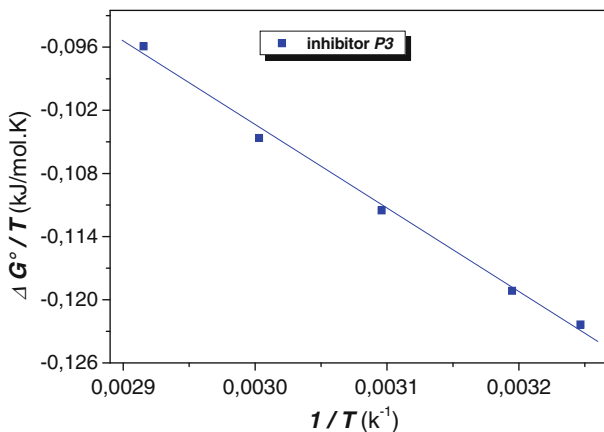

Fig. 7 Relationship between $\Delta G^{\circ}_{\text{ads}}/T$ and the inverse of absolute temperature
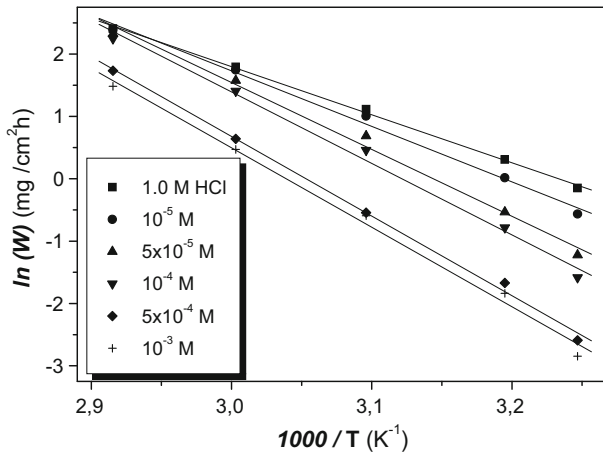
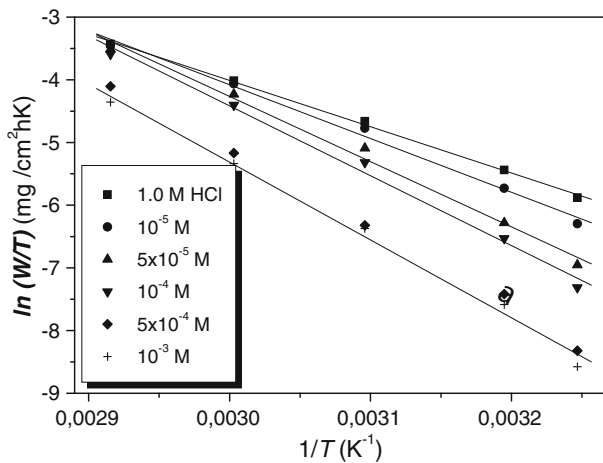**Fig. 8** Arrhenius plots for steel, for different concentrations of P3 in 1.0 M HCl

Fig. 9 The relationship between ln (W/T) and 1/T for inhibition of steel in 1.0 M HCl containing different concentrations of P3

The E_a for the corrosion reaction in the absence and presence of different concentrations of the inhibitor P3 was calculated. The values of E_a depend on inhibitor concentration. On the other hand, the plots of ln (W/T) against 1/T (Eq. 12) also gave straight lines with correlation coefficients (r) in the range 0.9959–0.9990 (average: 0.9970), as shown in Fig. 9. The slopes of these lines equals $-\Delta H^*/R$ and the intercept is ln $(RT/N_A h) + (-\Delta S^*/R)$, from which the values of ΔH^* and ΔS^* were calculated. Kinetic data obtained from these graphs are given in Table 4.

Some studies [41–43] have shown that compared with the apparent activation energy in the absence of inhibitor, higher values for E_a were found in the presence of inhibitors. Other studies [44, 45] have shown that in the presence of inhibitors the

apparent activation energy was lower than that in the absence of inhibitors. However, other research has shown that at low inhibitor concentrations the values of E_a were higher in the presence of inhibitor than in the absence of inhibitor, whereas at high inhibitor concentrations the values of E_a were lower than those in the uninhibited acid solution [46].

The value of the apparent activation energy E_a of the hydrogen evolution reaction for 1.0 M HCl without an inhibitor (64.133 kJ mol^{-1}) (Table 5) agrees well with literature data on E_a for iron and steel in hydrochloric acid, which are in the range 58–88 kJ mol^{-1}, and most are grouped around 60.7 kJ mol^{-1} [47–49]. Addition of inhibitor modified the values of the apparent activation energies; this modification may be attributed to the change in the mechanism of the corrosion process in the presence of adsorbed inhibitor molecules [50]. The lower value of the activation energy of the process in an inhibitor's presence compared to that in its absence is attributed to its chemisorption, whereas the opposite is the case with physical adsorption [51, 52].

It is apparent from Table 5 that the values of apparent activation energy E_a are higher in the presence of inhibitor than in its absence (64.133 kJ mol^{-1}). This type of inhibitor retards corrosion at ordinary temperatures but inhibition is diminished at elevated temperatures.

As can be seen in Table 5, the values of the pre-exponential factor A increase continuously as the concentration increases, and it is the combined effect of the frequency factor A and E_a that dictate the rate of steel dissolution. It was clear that from this study that the values of A and E_a in the presence of P3 are higher than those of in the uninhibited acid solution. These results are in accord with reported studies [43, 53]. As such the corrosion rate is found to be lowest at a concentration of P3 of 10^{-3} M, even though it has the highest E_a. We remark also (Fig. 10) that when the inhibitor concentration reached 5×10^{-4} M, the values of E_a reach a maximum and then do not change obviously. That is, the apparent activation energy acts as a function of inhibitor concentration [32].

The positive signs of ΔH^* reflect the endothermic nature of the steel dissolution process. The values of E_a and ΔH^* increase with increasing concentration of P3, suggesting that the energy barrier of corrosion reaction increases as the concentration of P3 is increased. This means that the corrosion reaction will further be

Table 5 Activation data and pre-exponential factor (A) of the dissolution reaction of steel in 1.0 M HCl solution containing different concentrations of P3

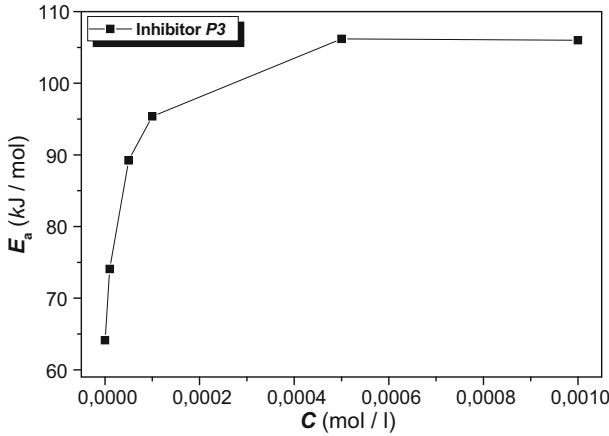| Inhibitor P3	Pre-exponential factor A (mg cm^{-2} h^{-1})	E_a (kJ mol^{-1})	ΔH^* (kJ mol^{-1})	ΔS^* (J mol^{-1})
Blank	6.6659×10^{10}	64.13	61.43	−46.8
10^{-5}	2.2472×10^{12}	74.07	71.37	−17.5
5×10^{-5}	4.4269×10^{14}	89.24	86.54	26.4
10^{-4}	3.4882×10^{15}	95.38	92.69	43.6
5×10^{-4}	8.3616×10^{16}	106.18	103.48	70.1
10^{-3}	6.5405×10^{16}	106.00	103.30	68.0

Fig. 10 The relationship between E_a and inhibitor concentration of P3

pushed to surface sites that are characterized by progressively higher values of E_a as the concentration of the inhibitor becomes greater [40].

In this study, it was found that ΔS^* increases with increasing concentration of P3, and passes from -17.5 J mol^{-1} at 10^{-5} M to 68.2 J mol^{-1} at 10^{-3} M, furthermore, we notice that ΔS^* changes its sign from negative to positive as a result of a possible change in the mechanism of the corrosion process. This result was similar to the author's previous outcome [54].

Effect of hydrochloric acid concentration on inhibition efficiency

Figure 11 shows the effect of HCl concentration (1–10 M) at 35 °C on the inhibition efficiency of P3 at 10^{-3} M. The increasing hydrochloric acid concentration resulted in decreasing E_w, and the maximum efficiency was 93% in 1 M HCl.
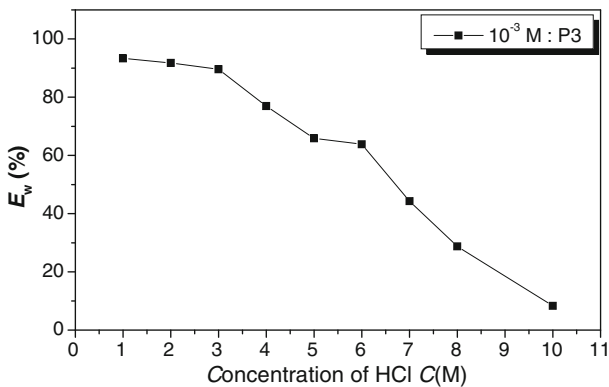

Fig. 11 Effect of HCl concentration on E_W (%) of P3 for the steel at 35 °C

Figure 11 also clearly shows that the change of E_w with HCl concentration can be divided into four stages. We notice also that in the two domains of concentration 1–3 M and 5–6 M E_w decreases slightly with acid concentration; but in the ranges of acid concentration 3–5 M and 6.0–10 M the inhibition efficiency decreases substantially with acid concentration.

Rate constant and reaction constant

Assuming the corrosion rate against the molar concentration of acid concentration obeys the expression proposed by Mathur and Vasudevan [55],

$$\ln W = \ln k + BC \tag{13}$$

where k is the specific reaction rate constant, B is a constant for the reaction, and C is the molar concentration of HCl.

Figure 12 shows the relationship between $\ln W$ and C. It is seen clearly that the graph of $\ln W$–C in uninhibited HCl is a straight line. After P3 is added, however, two straight lines appear, with a break point at 4 M HCl. Calculated kinetic data are listed in Table 6.

Equation 13 shows that k can be regarded as an initial rate at zero acid concentration, so k means the corrosive ability of HCl for steel [53, 55, 56]. Table 6
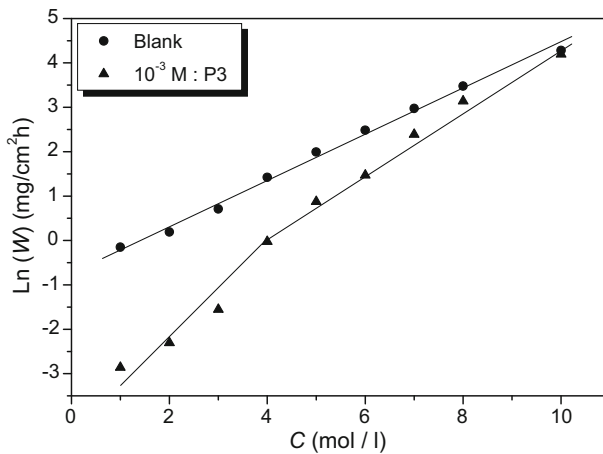

Fig. 12 Variation of $\ln W$ with the concentration of hydrochloric acid, C, at 35 °C

Table 6 Calculated values of kinetic data for the corrosion of steel in HCl containing P3 at 35 °C

Concentration	B (mg cm^{-2} h^{-1} M^{-1})		k (mg cm^{-2} h^{-1})	
	1–4 M HCl	4–10 M HCl	1–4 M HCl	4–10 M HCl
Blank	0.5156	0.5156	0.4948	0.4948
10^{-3} M	0.91942	0.7102	0.0185	0.0656

clearly shows that k decreases obviously after P3 is added to the HCl solution, which indicates that P3 is a good inhibitor in HCl. Furthermore, the values of k in 1–4 M HCl inhibited solution are smaller than those in 4–10 M inhibited HCl solution, which indicates that the values of E_w (%) in 1–4 M HCl are larger than those in 4–10 M HCl (Fig. 12).

According to Eq. 13, B is the slope of the line ln W–C, so B indicates the changed extent of W with acid concentration. Values of B in inhibited HCl are higher than in uninhibited HCl, which indicates that the changed extent of W with C in inhibited HCl is bigger than that in uninhibited HCl. Namely, the inhibition efficiency decreases obviously with acid concentration (Fig. 12). In addition, the values of B in 1–4 M inhibited HCl solution are higher than those in 4–10 M inhibited HCl solution, which indicates that the change of E_w (%) in 1–4 M HCl is greater than that in 4–10 M HCl.

Electrochemical impedance spectroscopy (EIS)

The impedance diagrams obtained after 30 min of exposure of the samples at 308 K in inhibited and uninhibited solutions containing different concentration of P3 are shown in Fig. 13. It is apparent from these plots that the impedance response of steel in uninhibited HCl solution has significantly changed after addition of P3 to the corrosive solution. This indicates that the impedance of inhibited substrate increases with increasing inhibitor concentration and, consequently, the inhibition efficiency increases. The locus of the Nyquist plots was regarded as one part of a semicircle. The impedance diagrams obtained are not perfect semicircles and this difference has been attributed to frequency dispersion [57, 58].

The impedance data such as the double-layer capacitance (C_{dl}), the charge-transfer resistance (R_t) and E_{R_t} (%) derived from Nyquist diagrams are given in Table 7.

The charge-transfer resistance, R_t, values are calculated from the difference in impedance at low and high frequencies, as suggested by Tsuru and Haruyama [59]. To obtain the double capacitance (C_{dl}), the frequency at which the imaginary
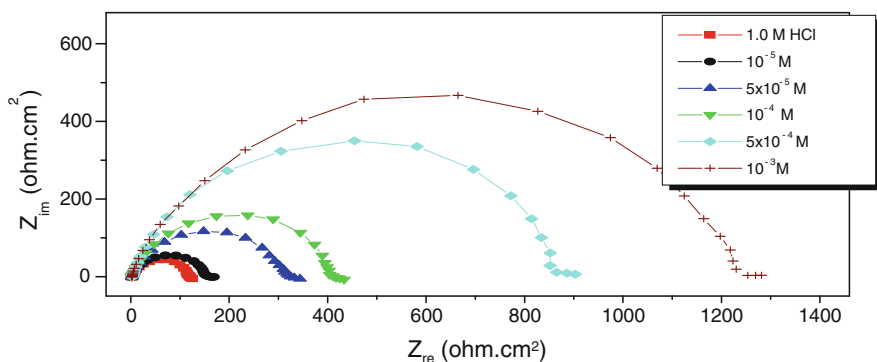

Fig. 13 Nyquist diagrams for steel in 1.0 M HCl containing different concentrations of P3

Table 7 Characteristic data evaluated from the impedance diagram for steel in 1.0 M HCl containing different concentrations of P3

Inhibitor	Concentration (M)	R_t (Ω cm^2)	f_{max} (Hz)	C_{dl} (μF/cm^2)	E_{R_t} (%)
Blank	1	115	15.82	87.51	–
	10^{-5}	154	17.857	57.90	25
	5×10^{-5}	312	10	51.04	63
	10^{-4}	405	7.937	49.54	72
	5×10^{-4}	867	4.464	41.14	87
	10^{-3}	1234	4	32.26	91
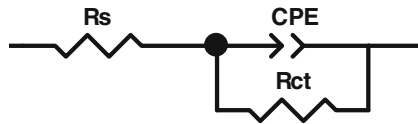
Fig. 14 Electrical equivalent circuit used for modeling the interface steel/1 M HCl solution without and with inhibitor

component of the impedance is maximum $(-Z_{max})$ is found and C_{dl} values are obtained from the equation:

$$f\left(-Z_{max}\right) = \frac{1}{2\pi C_{dl} R_t} \tag{14}$$

The inhibition efficiency from the charge-transfer resistance is calculated by use of the relationship:

$$E_{R_t}\% = \frac{R_{tcorr} - R_{tcorr}^{inh}}{R_{tcorr}} \times 100 \tag{15}$$

where R_{tcorr} and R_{tcorr}^{inh} are the charge transfer resistance values without and with inhibitor, respectively. R_t is the diameter of the loop.

The recorded EIS spectrum for steel in 1.0 M HCl, Fig. 13, shows one depressed capacitive loop in the absence and presence of P3 (one time-constant in Bode-phase representation). Addition of increasing concentrations of inhibitor increases the diameter of the capacitive loop, indicating inhibition of the corrosion process. In other words, R_{ct} increases and consequently enhances IE% until reaching their maximum values at 10^{-3} M ($E_{R_t}\% = 91$). The equivalent circuit for mild steel in molar HCl is widely discussed in the literature (Fig. 14) [60, 61]. The values of the double-layer capacitance (C_{dl}) tend to decrease. The decrease in the C_{dl} values is because of adsorption of the inhibitor on the metal surface [62].

Theoretical calculations

The calculated quantum chemical indices (E_{HOMO} = energy of the highest occupied molecular orbital, E_{LUMO} = energy of the lowest unoccupied molecular orbital) of

**Table 8** Partial total atomic charges calculated by the PETRA software [61]

Compound	N(1)	N(2)	NH$_2$	N(3)	N(4)	E_{HOMO} (eV)	E_{LUMO} (eV)	ΔE (eV)
P1	+0.0421	−0.3326	–	–	–	−9.305	+0.950	−10.255
P2	+0.0461	−0.3561	−0.2437	–	–	−8.632	+0.953	−9.585
P3	+0.0654	−0.3849	–	+0.1119	−0.3098	−8.577	+0.371	−8.948
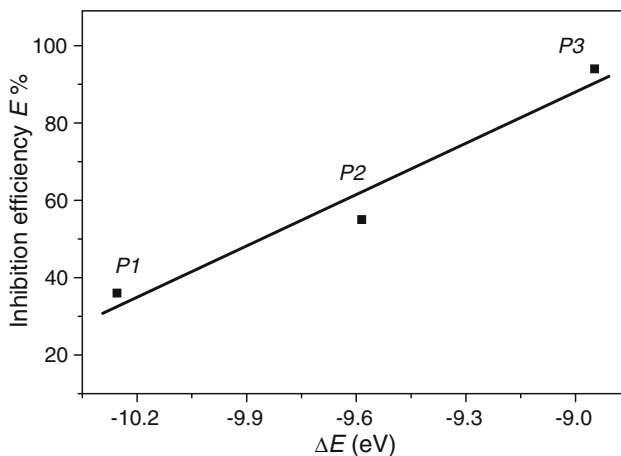
Fig. 15 Correlation of energy differences ΔE with percentage inhibition by pyrazole derivatives

the three inhibitors are shown in Table 8. Inhibition efficiency increases with increasing values of E_{HOMO} [63–66]. The results seem to indicate that charge transfer from the inhibitor takes place during adsorption on the metal surface. Increasing values of the E_{HOMO} may facilitate adsorption (and therefore inhibition) by affecting the transport process through the adsorbed layer. However, the difference $\Delta E = E_{HOMO} - E_{LUMO}$ is a negative number, whereas the coefficient of Δ is positive, indicating that a smaller absolute value of Δ, and therefore, a lower excitation energy to move an electron from the highest occupied molecular orbital, will cause higher inhibition efficiency. This means that the band gap energy value (Fig. 15) is more favourable for P3 than P1 and P2, which explains the percentage inhibition efficiency.

Table 8 indicates that for compound P3 only N(2) and N(4) have negative charges and, consequently, they are the centres of the adsorption phenomenon. N(1) and N(3) with positive charges do not participate in the adsorption process. The findings obtained by the experimental study and from calculation of the total partial charge on atoms of inhibitor P3 may suggest the adsorption mode as below (Scheme 2):

Scheme 2 Schematic representation of the mode of adsorption of P3
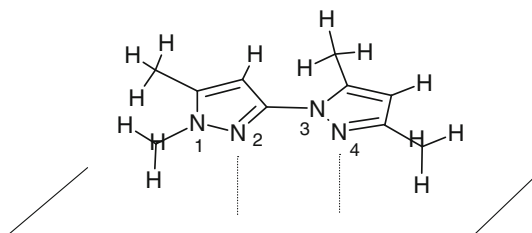
Conclusion

From the above results and discussion, the following conclusions are drawn.

- Inhibition efficiency increases with inhibitor concentration, and the best performance is seen for P3.
- P3 acts as a cathodic-type inhibitor.
- The adsorption of P3 on the steel surface from 1.0 M HCl obeys a Langmuir adsorption isotherm. The adsorption process is a spontaneous and exothermic process accompanied by a decrease in entropy.
- The efficiency of inhibition by P3 is temperature-dependent and its addition leads to an increase of the activation energy of the corrosion process. The adsorption equilibrium constant (k) decreases with increasing temperature.
- Calculated thermodynamic data reveal that the mechanism of adsorption of P3 on steel in 1.0 M HCl solution was typical of chemisorption.
- High E_{HOMO} and low energy gap ($E_{HOMO} - E_{LUMO}$) explain the best inhibition efficiency of P3.
- The results obtained from weight loss, potentiodynamic polarization, and impedance spectroscopy are in good agreement.

References

1. G. Trabanelli, Corrosion **47**, 410 (1991)
2. F. Bentiss, M. Traisnel, M. Lagrenée, Corros. Sci. **42**, 127 (2000)
3. S.A. Abd El-Maksoud, Appl. Surf. Sci. **206**, 129 (2003)
4. F. Bentiss, M. Lagrenée, M. Traisnel, J.C. Hornez, Corros. Sci. **41**, 789 (1999)
5. S. Kertit, B. Hammouti, Appl. Surf. Sci. **93**, 59 (1996)
6. A.A. El-Shafei, M.N.H. Moussa, A.A. El-Far, Mater. Chem. Phys. **70**, 175 (2001)
7. M.A. Quraishi, F.A. Ansari, D. Jamal, Mater. Chem. Phys. **77**, 687 (2002)
8. A. Aouniti, B. Hammouti, M. Brighli, S. Kertit, F. Berhili, S. El Kadiri, A. Ramdani, J. Chim. Phys. **93**, 1262 (1996)
9. M. Abdallah, M.M. El Naggar, Mater. Chem. Phys. **71**, 291 (2001)
10. M. Bouklah, A. Attayibat, B. Hammouti, A. Ramdani, S. Radi, M. Benkaddour, Appl. Surf. Sci. **240**, 341 (2005)
11. K. Tebbji, H. Oudda, B. Hammouti, M. Benkaddour, M. El Kodadi, F. Malek, A. Ramdani, Appl. Surf. Sci. **241**, 326 (2005)

12. F. Touhami, A. Aouniti, S. Kertit, Y. Abed, B. Hammouti, A. Ramdani, K. El Kacemi, Corros. Sci. **42**, 929 (2000)
13. A. Dafali, B. Hammouti, R. Touzani, S. Kertit, A. Ramdani, K. El Kacemi, Anticorros. Methods Mater. **49**, 96 (2002)
14. M. Benabdellah, R. Touzani, A. Aouniti, A. Dafali, S. El Kadiri, B. Hammouti, M. Benkaddour, Mater. Chem. Phys. **105**, 373 (2007)
15. A. El-Ouafi, B. Hammouti, H. Oudda, S. Kertit, R. Touzani, A. Ramdani, Anticorros. Methods Mater. **49**, 199 (2002)
16. K. Tebbji, H. Oudda, B. Hammouti, M. Benkaddour, M. El Kodadi, A. Ramdani, Colloids Surf. A Physicochem. Eng. Aspects **259**, 157 (2005)
17. M. Elayyachy, M. El Kodadi, B. Hammouti, A. Ramdani, A. El Idrissi, Pigment Res. Technol. **33**, 375 (2004)
18. S. Ramesh, S. Rajeswari, S. Maruthamuthu, Appl. Surf. Sci. **229**, 214 (2004)
19. A.B. Tadros, B.A. Abdenaby, J. Electroanal. Chem. **246**, 433 (1988)
20. R. Salghi, L. Bazzi, B. Hammouti, A. Bouchtart, S. Kertit, Z.A. Ait Addi, Z. El Alami, Ann. Chim. Sci. Mater. **25**, 187 (2000)
21. F. Chaouket, B. Hammouti, S. Kertit, K. El Kacemi, Bull. Electrochem. **17**, 311 (2001)
22. A. Ramdani, G. Tarrago, Tetrahedron **37**, 987–990 (1981)
23. A. Attayibat, S. Radi, A. Ramdani, Y. Lekchiri, B. Hacht, M. Bacquet, S. Willai, M. Morcellet, Bull. Korean Chem. Soc. **27**, 1648–1650 (2006)
24. L.L. Shreir, R.A. Jarman, G.T. Burstein, *Corrosion, vol. 2 (Chapter 20)* (Butterworth–Heinemann, Oxford, 1994), pp. 23–26
25. N. Hackerman, J.D. Sudbury, J. Electrochem. Soc. **94**, 4 (1950)
26. N. Hackerman, Corrosion **18**, 332 (1962)
27. X.L. Cheng, H.Y. Ma, S.H. Chen, R. Yu, X. Chen, Z.M. Yao, Corros. Sci. **41**, 321 (1999)
28. B.G. Ateya, B.E. El-Anadouli, F.M. El-Nizamy, Corros. Sci. **24**, 509 (1984)
29. K.F. Khaled, M.A. Amin, Corros. Sci. **51**, 1964 (2009)
30. I. Ahamad, R. Prasad, M.A. Quraishi, J. Solid State Electrochem. **14**, 2095 (2010)
31. L.B. Tang, G.N. Mu, G.H. Liu, Corros. Sci. **45**, 2251 (2003)
32. T.P. Zhao, G.N. Mu, Corros. Sci. **41**, 1937 (1999)
33. G.N. Mu, X.M. Li, F. Li, Mater. Chem. Phys. **86**, 59 (2004)
34. E. Khamis, Corrosion **46**, 476 (1990)
35. F.M. Donahue, K. Nobe, J. Electrochem. Soc. **112**, 886 (1965)
36. E. Khamis, F. Bellucci, R.M. Latanision, E.S.H. El-Ashry, Corrosion **47**, 677 (1991)
37. W. Durnie, R.D. Marco, A. Jefferson, B. Kinsella, J. Electrochem. Soc. **146**, 1751 (1999)
38. S. Martinez, I. Stern, Appl. Surf. Sci. **199**, 83 (2002)
39. M.K. Gomma, M.H. Wahdan, Mater. Chem. Phys. **39**, 209 (1995)
40. I. Putilova, S. Balezin, V. Barannik, *Metallic Corrosion Inhibitors* (Pergamon Press, Oxford, 1960)
41. S.T. Arab, E.A. Noor, Corrosion **49**, 122 (1993)
42. M. Elachouri, M.S. Hajji, M. Salem, S. Kertit, J. Aride, R. Coudert, E. Essassi, Corrosion **52**, 103 (1996)
43. E.S. Ferreira, C. Giacomelli, F.C. Giacomelli, A. Spinelli, Mater. Chem. Phys. **83**, 129 (2004)
44. S.N. Banerjee, S. Misra, Corrosion **45**, 780 (1989)
45. Q.H. Cai, Y.K. Shan, B. Lu, X.H. Yuan, Corrosion **49**, 486 (1993)
46. S.A. Ali, A.M. El-Shareef, R.F. Al-Ghamdi, M.T. Saeed, Corros. Sci. **47**, 2659 (2005)
47. A. Popova, E. Sokolova, S. Raicheva, M. Christov, Corros. Sci. **45**, 33 (2003)
48. O. Riggs, I.R. Hurd, M. Ray, Corrosion **23**, 252 (1967)
49. Q.I.M. Sulaiman, H.M. Al-Saaty, in *Proc. of the 7 SEIC, Ann. Univ.* Ferrara., Italy, Sez. 5, Suppl. No. 9, 1990, p. 189
50. B. Mernari, L. Elkadi, S. Kertit, Bull. Electrochem. **17**, 115 (2001)
51. T. Szauer, A. Brandt, Electrochim. Acta **26**, 1253 (1981)
52. Z.A. Foroulis, in *Proceedings of the 6th European Symposium on Corrosion Inhibitors*, Ferrara, 1985, p. 48
53. G. Mu, X. Li, J. Colloid Interface Sci. **289**, 184 (2005)
54. S.S. Abd El Rehim, M.A.M. Ibrahim, K.F. Khalid, Mater. Chem. Phys. **70**, 268 (2001)
55. P.B. Mathur, T. Vasudevan, Corrosion **38**, 171 (1982)
56. L. Wang, G.J. Yin, J.G. Yin, Corros. Sci. **43**, 197 (2001)
57. F. Mansfeld, M.W. Kending, S. Tsai, Corrosion **37**, 301 (1981)

58. F. Mansfeld, M.W. Kending, S. Tsai, Corrosion **38**, 570 (1982)
59. T. Tsuru, S. Haruyama, B. Gijutsu, J. Jpn. Soc. Corros. Eng. **27**, 573 (1978)
60. A. Abdel Nazeer, A.S. Fouda, E.A. Ashour, J. Mater. Environ. Sci. **24**, 24 (2011)
61. M. Kissi, M. Bouklah, B. Hammouti, M. Benkaddour, Appl. Surf. Sci. **252**, 4190 (2006)
62. A. Chetouani, K. Medjahed, K.E. Sid-Lakhdar, B. Hammouti, M. Benkaddour, A. Mansri, Corros. Sci. **46**, 2421 (2004)
63. M. Mihit, K. Laarej, H. Abou El Makarim, L. Bazzi, R. Salghi, B. Hammouti, Arab. J. Chem. **3**, 55 (2010)
64. M. Lagrenée, B. Mernari, N. Chaibi, M. Traisnel, H. Vezin, F. Bentiss, Corros. Sci. **43**, 951 (2001)
65. L. Herrag, B. Hammouti, S. Elkadiri, A. Aouniti, C. Jama, H. Vezin, F. Bentiss, Corros. Sci. **52**, 3042 (2010)
66. W.-D. Ihlenfeldt, J. Gasteiger, J. Comput. Chem. **8**, 793 (1994)